Published in final edited form as:
J Vasc Interv Radiol. 2010 November ; 21(11): 1708–1715. doi:10.1016/j.jvir.2010.06.024.

Vascular smooth muscle cells ablation with endovascular non thermal irreversible electroporation

Elad Maor[1], **Antoni Ivorra**[2], **James J. Mitchell**[3], and **Boris Rubinsky**[1,4]

[1] Biophysics Graduate Group, University of California, Berkeley, California

[2] Department of Information and Communication Technologies, Universitat Pompeu Fabra

[3] Angiodynamics Inc., Queensberry, New-York

[4] Department of Mechanical Engineering, University of California, Berkeley, California

Abstract

Purpose—Using fundamental principles of electroporation and mathematical analyses of temperature and electrical fields of blood vessels we developed an endovascular ablation approach - non thermal irreversible electroporation (NTIRE). The purpose of this study was to evaluate the effect of endovascular NTIRE on blood vessels.

Material and Methods—Specially made endovascular devices with four electrodes on top of inflatable balloons were used to apply electroporation pulses. Finite element simulations were used to characterize NTIRE protocols that will not induce thermal damage to treated tissues. Right iliac arteries of eight rabbits were treated with 90 NTIRE pulses. Angiograms were preformed before and after the procedures. Arterial specimens were harvested at 7 and 35 days. Evaluation included Hematoxylin & Eosin, elastic Von Giessen, and Masson's Trichrome stains. Immunohistochemistry of selected slides included smooth muscle actin, proliferating cell nuclear antigen, von willebrand factor and S-100 antigen.

Results—At 7 days, all NTIRE-treated arterial segments displayed complete, transmural ablation of vascular smooth muscle cells (VSMC). At 35 days, similar damage to VSMC was noted. In most cases, elastic lamina remained intact and endothelial layer regenerated. Occasional mural inflammation and cartilaginous metaplasia were noted. After five weeks there was no evidence of significant VSMC proliferation, with the dominant process being wall fibrosis with regenerated endothelium.

Conclusions—NTIRE can be applied in an endovascular approach. It efficiently ablates vessel wall within seconds and with no damage to extra-cellular structures. NTIRE has possible applications in many fields of clinical cardiology, including arterial restenosis and cardiac arrhythmias.

INTRODUCTION

Catheter ablation is finding increasing use in modern medicine.(1) Current ablation strategies include thermal ablation (with high or low temperatures)(5–7), ethanol injection(1) and photodynamic therapy(8). Characteristic of all approaches is the indiscriminant destruction of

Contact: Dr. Elad Maor, MD PhD, 6124 Etcheverry Hall, Mailing Code: 1740, Department of Mechanical Engineering, University of California, Berkeley, CA-94720, Telephone/Fax: (510)643-1866, eladmaor@gmail.com.

both cells and extra-cellular structures within the ablated volume.(8,9) Non-thermal irreversible electroporation (NTIRE) is a non-thermal, non pharmacological, electric ablation technique based on the biophysical phenomenon of electroporation. When cells are exposed to a sufficiently high external electric field, nano-scale aqueous pores are created in the cells' phospholipid bilayer.(10) Electroporation is associated with a significant increase in electrical conductivity and molecular transport across the cells' membrane phospholipid bilayer.(11, 12) When the damage to the phospholipid bilayer is significant cells experience a loss in intracellular homeostasis and die, in a phenomenon called irreversible electroporation. Irreversible electroporation has been successful in ablating soft tissues in animal models and was also shown to attenuate neointimal formation in a rodent carotid artery injury model. (13–19) This study evaluates NTIRE as an endovascular ablation modality. Particular to our approach is that the electrical pulses are designed to avoid any elevation of temperature that may cause thermal damage (20) and to find ways to deliver these pulses from the interior of blood vessels. Here we simulate assemble and test for the first time an endovascular NTIRE prototype, and evaluate *in-vivo* its short and long term effect on the walls of iliac arteries of New-Zealand white rabbits.

MATERIAL AND METHODS

Endovascular device assembly

The endovascular device used in this study is shown in Figure 1. We assembled and simulated alternative geometries, some failed for different reasons. Here we are presenting the best design only. The catheter shaft consisted of a 0.5 mm diameter nickel titanium (NiTi) tube electrically insulated with a layer of polyimide and polyethylene terephthalate. Rectangular nickel titanium wire with cross sectional dimensions of 0.5 mm × 0.1 mm and an active length of 20 mm was used as the electrodes, with a bipolar design of 4 separate electrodes. The electrodes were orientated parallel to the axis of the balloon and evenly spaced in a radial pattern around the circumference of the balloon. The electrodes were positioned over a standard polyethylene terephthalate non-compliant balloon with an expanded diameter of 2.5 mm and a length of 20 mm.

Finite element simulations

The governing equations with a solution for a single electroporation pulse were described elsewhere with needles and with parallel plates geometries.(20,21) In brief, the Joule heating is evaluated by solving the Laplace equation for potential distribution:

$$\nabla \cdot (\sigma \nabla \phi) = 0 \tag{1}$$

$$\nabla \cdot (\mathrm{k}\nabla \mathrm{T}) + \omega_{\mathrm{b}} c_{\mathrm{b}} (\mathrm{T_a} - \mathrm{T}) + \mathrm{p} = \rho \mathrm{c_p} \frac{\partial \mathrm{T}}{\partial \mathrm{t}} \tag{2}$$

where ϕ is the electric potential (volts), σ is the electrical conductivity (0.6 S/m) and p is the heat generation rate per unit volume (W/m^3). The heating of the tissue resulting from electroporation can be calculated by adding the Joule heating source term to the Pennes bio-heat transfer equation:

$$\nabla(k\nabla T) + \omega_b c_b (T_a - T) + \sigma |\nabla \phi|^2 = \delta \rho c_p \frac{\partial T}{\partial t} \tag{3}$$

where k is the thermal conductivity of the tissue (0.5 W/m K), T is the absolute temperature, ω_b is the blood perfusion rate (0.0005 s^{-1}), c_b is the heat capacity of the blood (3640 J/Kg K), Ta is the arterial temperature (273.15 K), ρ is the tissue density (1,000 Kg/m3) and c_p is the heat capacity of the tissue (3,750 J/Kg K). All constants are based on previously published literature.(20,22–24)

Using the transient temperature solution of equation (3), a kinetic model of thermal damage base on the Arrhenius formulation can be used.(25) The model calculates the Henriques and Moritz thermal damage integral:

$$\Omega(t)=\int Ae^{-\frac{E}{RT}}dt \tag{4}$$

where T is the transient temperature from equation (3), Ω is a dimensionless indicator of damage, A is a measurement of molecular collision frequency (5.6×10^{63} s^{-1}), E is an energy barrier that molecules surmount in order to denature (4.3×10^{5} J/mol), R is the gas constant (8.314 J/mol K) and t is the time (s). The values of A and E are unique and are based on experiments in different tissue evaluating different kinds of damage. Our analysis is based on values of A and E that are appropriate for thermal damage of human arterial tissue.(26) All values of Ω in our analysis refer to the maximal value of the thermal integral, based on the maximal temperature in each time evaluation point.

The dimensionless indicator of thermal damage, Ω, is a function of two process parameters (molecular collision frequency and energy barrier) together with the transient analysis of temperature. In fact, Ω is the logarithm of the relative concentration of “reactants”:

$$\Omega(\mathrm{T})=\ln\frac{\mathrm{C}(0)}{\mathrm{C}(\mathrm{T})} \tag{5}$$

where C(0) and C(T) are the amount of native (undamaged) molecules in time zero and T, respectively. Therefore at Ω =1, a standard point of comparison 63.2% of the molecules in the arterial wall have already been changed into damaged state. (25) Equation (5) can also be presented in a different way to describe the fraction of damaged molecules:

$$F_d=1-\frac{c(\tau)}{c(0)}=1-e^{-\Omega} \tag{6}$$

Electroporation pulses are discrete square DC pulses of length t_1, with a pulse frequency rate of f. Thermal damage analysis takes into account both the resistive heating during the pulses, as well as the time interval with no resistive heating between the pulses. For multiple pulse electroporation protocols, the problem is solved separately for each time interval (either pulse or inter-pulse pause), with the transient solution at the end of the time-interval used as the initial condition for the next time-interval:

$$\Omega(t)=\sum_{i=0}^{N-1}\left(\int_{i\tau}^{i\tau+t_1}Ae^{-\frac{E}{RT}}dt+\int_{i\tau+t_1}^{i\tau+t_1+t_2}Ae^{-\frac{E}{RT}}dt\right) \tag{7}$$

where N is the total number of electroporation pulses, t_1 is the pulse duration interval, t_2 is the time interval between the end of the pulse and the beginning of the next pulse, and T is the sum of t_1 and t_2. The frequency of the electroporation protocol is defined as:

$$f=\frac{1}{T} \tag{8}$$

Boundary conditions

The problem was modeled as a hollow tube (artery) inside a large homogenous tissue block, with the endovascular electrodes located on the inner surface of the hollow tube. For the electric potential equation, the electrodes were represented by a fixed voltage (Dirichlet) boundary condition, with one electrode having a positive potential and the other one set to zero:

$$\phi_1=V_0 \tag{9}$$

$$\phi_2=0 \tag{10}$$

where Vo is the potential difference (volts) applied across the electrodes during the electroporation pulses. Zero electric flux (Neumann) boundary condition was applied at all the boundaries of the model not in contact with the electrodes:

$$\frac{\partial\phi}{\partial n}=0 \tag{11}$$

For the bio-heat equation, initial temperature in the entire domain was set to the physiologic temperature (273.15°K). The boundaries along the hollow tube were taken to be adiabatic (Neumann) boundary conditions to predict the maximal temperature rise along the arterial wall:

$$\frac{\partial T}{\partial n}=0 \tag{12}$$

The outer surface of the large tissue block was defined as constant physiological temperature (Dirichlet) boundary condition:

$$T=310.15^{\circ}K \tag{13}$$

In-vivo experiments

Eight New-Zealand white rabbits weighing 3.6–4.6 Kg were used in this study. Animals received humane care from a properly trained professional in compliance with both the Principals of Laboratory Animal Care and the Guide for the Care and Use of Laboratory Animals, published by the National Institute of Health. Institutional animal care and use commity approval was obtained prior to performing the animal experiments. Ketamine (35mg/kg body weight) and xylazine (5 mg/kg body weight) were used for anesthesia induction, followed by endotracheal intubation and isoflurane for anesthesia maintenance. A single pancuronium dose (0.1mg/kg) was used to attenuate muscle contractions. Animals were monitored continuously (oxygen saturation, ECG monitor, blood pressure, respiratory rate, CO2 production and core body temperature), and were under full heparinization during the entire procedure (heparin loading dose of 75–100 mg/Kg followed by ACT monitoring at 2–2.5× baseline levels using heparin.). Under sterile technique, the area over the right femoral

artery was exposed. Arteriotomy was performed, and a 4F introducer was placed in the right femoral artery.

The endovascular IRE device was inserted in a retrograde manner to the iliac artery of all animals. Using angiography guidance, the catheter was advanced to the aortic bifurcation, and inflated along the first two centimeters of the right iliac artery. IRE protocol in all animals included 90 pulses of 100 μs at 4 Hz frequency. Potential difference was 600 volts. Pulses were applied using a high voltage pulse generator intended for electroporation procedures (ECM 830, Harvard Apparatus, Holliston, MA). Current and voltage were recorded by means of special oscilloscope probes (current probe was AP015 and high voltage probe was ADP305, both from LeCroy Corp.). From these two signals electrical conductance was obtained during the pulses.

ECG was recorded and printed before, during and immediately after the procedure. After removal of the balloon device, control angiography was performed to confirm patency of the vessel and to rule out any local bleeding of the treated artery. At the end of the procedure, the femoral artery was ligated, and the surgical wound was closed. In all eight animals, the left iliac artery served as a control artery, and did not undergo any intervention. Animals recovered and were kept in the animal facility for follow up. Animals received anti platelets therapy (Clopidogrel) after the procedure and during the follow up period.

A follow up period of 7 days was used for four animals, and a period of 35 days was used for the remaining four animals. At the end of the follow up period, animals were anesthetized as described above, euthanized with an overdose of pentobarbital, and the arterial vasculature was perfused with formalin. For all animals, both iliac arteries (3cm segments starting from the aortic bifurcation) were harvested and sent to histology for processing and evaluation.

Histology

Formalin-fixed, 3 cm long intact segments of the left and right iliac arteries from eight rabbits were submitted for evaluation by an independent pathology laboratory (Charles River Laboratories Pathology Associates). Six consecutive sections were prepared from each of the right iliac arteries, and three consecutive sections were prepared from each of the left iliac arteries. The tissues were processed through and embedded in paraffin. From each paraffin block, three 5 μm sections were prepared and stained with hematoxylin & eosin (H&E), Masson's trichrome (MT), and Verhoeff's elastin (VE) stains. The sections were evaluated microscopically by an independent veterinary pathology (Charles River Laboratories Pathology Associates), who was blinded with respect to the treatment. For each artery segment, two parameters were evaluated: mural damage (i.e. VSMC ablation) and inflammation. The distribution (portion of the section circumference affected) and severity of the changes were scored. Distribution score for both parameters were based on the following: 0 = no change; 1 = Less than 10%; 2 = 10%–24%; 3 = 25–75%; 4 = more than 75%. Mural damage scores were based on the following changes: 0 = no change; 1 = internal elastic lamina (IEL) fragmented or missing; 2 = less than 50% of VSMC affected; 3 = 50–75% of VSMC affected; 4 = >75% VSMC affected. Inflammation scores were based on the following: 0 = no inflammation; 1= minimal; 2 = mild; 3 = moderate; 4 = marked (severe). Selected sections (one control, one 7-day artery and two 35-days arteries) were processed and evaluated using immunohistochemisty. Evaluation included smooth muscle actin (mouse anti-smooth muscle actin, ZYMED laboratories, catalog #18-0106), proliferating cell nuclear antigen (monoclonal mouse anti proliferating cell nuclear antigen, DakoCytomation, catalog #M0879), von willebrand factor (sheep anti-human von willebrand factor, the binding site limited U.K., catalog #PC054) - a useful marker for endothelial cells, and sS-100 (mouse anti-S-100 monoclonal antibody, Millipore, catalog #MAB079-1) which is a useful marker for chondrocytes

RESULTS

Finite-element simulation

Finite-element simulation of an endovascular device prototype demonstrated that a potential difference of 600 volts induced an electric field of 1,000 volts per centimeter or above across the entire thickness of a typical iliac arterial wall (Figure 1). Ninety pulses of 100 microseconds at a frequency of 4 hertz demonstrated that the maximal temperature in the arterial wall did not exceed 66.8 °C, and that the average temperature did not exceed 61.7 °C, with a total treatment duration of 22.5 seconds. Analysis of the thermal damage integral based on the Arrhenius equation demonstrated that with the above described protocol, no significant thermal damage was induced within the arterial wall (Ω_{max}=0.012, corresponding to 1.59% thermally damaged molecules in areas of maximal temperature).

In-vivo experiments

In-vivo animal experiments showed no ECG changes with any of the animals. Control angiograms immediately after the procedures showed no acute occlusion or rupture of the vessels. All animals survived the follow up period, without infection bleeding or evidence of limb ischemia. On gross pathology NTIRE-treated arteries were not different from control arteries, and there was no evidence of local bleeding or thrombosis. Electrical conductance was recorded during each electroporation pulse with seven animals, by recording the voltage and the current during the application of the electric field. All seven observations demonstrated a slight, non significant increase in electrical conductance between the first and last electroporation pulse (0.013±0.003 Siemens at the first pulse versus 0.024±0.03 at the last pulse).

Histology at 7 days

Histology scores of mural damage (i.e. VSMC ablation) and local inflammation are summarized in Table 1, with representative images shown in Figures 2–5. All IRE-treated iliac artery segments displayed severe, transmural ablation of VSMC in at least five of the six segments. In nearly all sections the damage was circumferential. The damage to the tunica media was characterized by complete loss of VSMC, with intact collagen and elastic fibers becoming the only components of the tunica media layer. Endothelial cells repopulated the Tunica Intima, along the relatively intact internal elastic lamina. Most inflammatory reaction was perivascular (chronic). Left iliac artery segments were unremarkable.

Histology at 35 days

Histology scores of mural damage (i.e. VSMC ablation) and local inflammation are summarized in Table 1, with representative slide images shown in Figures 2–5. All NTIRE-treated iliac artery segments displayed circumferential damage in nearly all sections. Damage was characterized by persistent loss of VSMC, with the Tunica Media replaced with fibroblasts and fibrotic, collagenous tissue (figure 4 top right images, figure 3 top image). In most cases, elastic lamina remained intact (figure 2 right image, figure 3 top image). Occasional mural inflammation was noted (figure 5 right image). This included mononuclear cells (primarily) as well as polymorphonuclear cells (neutrophils). Most of the chronic inflammatory reaction was perivascular, but some of the segments showed inflammatory cells through the wall (not shown). Some of the treated arteries demonstrated asymmetrical, fibrous non-cellular neointima covering the intimal surface. In three sections out of total of 23 segments evaluated, small foci of cartilaginous metaplasia were noted (Figure 5 right image). Left iliac arteries (non-treated) were unremarkable.

Immunohistochemistry

Advanced histology results are summarized in Figures 4 and 5. Smooth muscle actin (SMA) stain was homogeneously positive in the Tunica Media of the control arteries, but was absent from all IRE-treated segments evaluated at 7 and 35 days (Figure 4, top row). Local areas of positive SMA were noticed in the small neointima covering the intimal surface of arteries evaluated at 35 days. Proliferating cell nuclear antigen (PCNA) stain was negative in the control arteries as well as in the 7-days segments (Figure 4, middle row). Positive PCNA stains were noted in the perivascular areas of the arteries evaluated at 35 days, as well as some mild positive stain within the Tunica Media itself. Von willebrand factor (VWF) lightly stained the endothelial layer of control arteries (Figure 4, bottom row). After one week, strong VWF staining of the cells lining the inner layer of the treated arteries was noted, although it was not continuous on all segments evaluated. After five weeks, the inner layer of the treated arteries showed homogeneous circumferential and strong VWF staining. Foci of cartilaginous metaplasia contained cells that stained positively for the S-100 antigen (Figure 5).

DISCUSSION

This report shows successful endovascular ablation with NTIRE. Our study demonstrates that endovascular NTIRE can efficiently ablate VSMC in the arterial wall with no damage to the extra-cellular components, with minimal inflammatory response, with limited proliferation of VSMC and with rapid repopulation of functional endothelial cells. Our results are supported by previous studies evaluating the effect of electric field on blood vessels. In previous work with rodent carotid arteries, 90 electroporation pulses of 1,750 V/cm induced ablation of more than 90% of the vascular smooth muscle cell population.(27) The results described here show that even lower electric fields were high enough to induce NTIRE.

The hallmark of NTIRE ablation is its effect on the phospholipid bilayer. By inducing long lasting aqueous pores, cells succumb to the drastic change in the intra-cellular environment. (28–30) Our results demonstrate that elastic fibers and extra-cellular collagen were preserved, and that extensive destruction of the cells did not induce failure of the wall integrity. In addition, endovascular NTIRE enabled fast regeneration of functional endothelium, probably from circulating endothelial progenitor cells. (31)

SMA staining at 35 days demonstrated limited repopulation of the ablated arteries with VSMC. These cells can be in two distinctive phenotypes: contractile or proliferative.(32) With the proper stimuli, VSMC can proliferate and create new blood vessels or significant neointima along stented arteries. However, in our study it seems that VSMC did not repopulate the arterial walls despite severe insult, and that a fibrotic healing was the dominant process. A plausible explanation is the minor damage to the collagen fibers. Koyama and colleagues showed that collagen suppresses smooth muscle cell proliferation and arrests them in G1.(33) Our study demonstrated that endovascular IRE did not damage the extra-cellular collagen fibers. Therefore, the intact collagen might have prevented VSMC proliferation, leaving the fibroblastic healing process as the only dominant post-IRE response.

In three of the 23 sections evaluated at 35 days foci of cartilaginous metaplasia were noticed. Those foci were confirmed with positive staining of the cells for the S-100 antigen, a characteristic antigen of chondorcytes.(34) Our finding is consistent with the reported plasticity of the adult smooth muscle cell phenotype and its role in vascular calcifications.(35,36,9) It is plausible that the three foci reported here are the result of transdifferentiation of surviving VSMC, triggered by paracrine effects and local inflammation. (37), (38)

With the properties described above and it short intervention time of 22.5 seconds, endovascular NTIRE lends itself to multiple cardiovascular applications. NTIRE has the

potential to prevent neointimal formation, (19) and is applicable to wide range of restenotic processes including post-angioplasty restenosis, in-stent restenosis, and dialysis access failure.. In addition, the sparing of extra-cellular matrix and the minimal inflammatory reaction enable NTIRE to ablate atrial tissue with reducied the likelihood of pulmonary vein stenosis or wall perforation, two complications of the currently used thermal ablation techniques.(9) Therfore, potential future applications of NITRE include in-stent restenosis, hemodialysis vascular access failure and cardiac arrhythmias ablation.

This is a preliminary study and much additional work would be needed to confirm our observations. Our immunohistochemistry work was preliminary and included only representative slides. We used only smooth muscle cell actin antibodies in order to identify vascular smooth muscle cells. However, this molecule appears also in myofibroblasts and therefore additional staining with myosin heavy chain isoform could have confirmed our observations. In addition, we used only masson's trichrome for fibrosis process evaluation on day 35. An additional study with Sirius Red stain for the evalution of collagen production is important to confirm this observation.

In conclusion, we presented here a nonthermal endovascular ablation approach. This approach is based on the biophysical phenomenon of electroporation. Our approach is simple, fast, causes minimal damage to the extra cellular scaffold and has many immediate applications in cardiovascular medicine.

References

1. Nattel S. New ideas about atrial fibrillation 50 years on. Nature 2002;415:219–226. [PubMed: 11805846]
2. Chen S, Hsieh M, Tai C, et al. Initiation of Atrial Fibrillation by Ectopic Beats Originating From the Pulmonary Veins: Electrophysiological Characteristics, Pharmacological Responses, and Effects of Radiofrequency Ablation. Circulation 1999;100:1879–1886. [PubMed: 10545432]
3. Seggewiss H, Gleichmann U, Faber L, Fassbender D, Schmidt HK, Strick S. Percutaneous transluminal septal myocardial ablation in hypertrophic obstructive cardiomyopathy: acute results and 3-month follow-up in 25 patients. J Am Coll Cardiol 1998;31:252–258. [PubMed: 9462563]
4. Gonska BD, Cao K, Schaumann A, Dorszewski A, von zur Muhlen F, Kreuzer H. Catheter ablation of ventricular tachycardia in 136 patients with coronary artery disease: results and long-term follow-up. J Am Coll Cardiol 1994;24:1506–1514. [PubMed: 7930283]
5. Jackman W, Beckman K, McClelland J, et al. Treatment of supraventricular tachycardia due to atrioventricular nodal reentry, by radiofrequency catheter ablation of slow-pathway conduction. N Engl J Med 1992;327:313–318. [PubMed: 1620170]
6. Manusama R, Timmermans C, Limon F, Philippens S, Crijns HJG, Rodriguez L. Catheter-Based Cryoablation Permanently Cures Patients With Common Atrial Flutter. Circulation 2004;109:1636–1639. [PubMed: 15023886]
7. Grundfest W, Litvack F, Forrester J, et al. Laser ablation of human atherosclerotic plaque without adjacent tissue injury. J Am Coll Cardiol 1985;5:929–933. [PubMed: 3838324]
8. Dolmans DE, Fukumura D, Jain RK. Photodynamic therapy for cancer. Nat Rev Cancer 2003;3:380–387. [PubMed: 12724736]
9. Taylor GW, Kay GN, Zheng X, Bishop S, Ideker RE. Pathological Effects of Extensive Radiofrequency Energy Applications in the Pulmonary Veins in Dogs. Circulation 2000;101:1736–1742. [PubMed: 10758058]
10. Weaver, JC.; Chizmadzhev, Y. Handbook of biological effects of electromagnetic fields. CRC Press; 2007. Electroporation; p. 293-332.
11. Neumann E, Schaefer-Ridder M, Wang Y, Hofschneider PH. Gene transfer into mouse lyoma cells by electroporation in high electric fields. The EMBO Journal 1982;1:841–845. [PubMed: 6329708]
12. Aihara H, Miyazaki J. Gene transfer into muscle by electroporation in vivo. Nat Biotech 1998;16:867–870.

13. Maor E, Ivorra A, Leor J, Rubinsky B. The Effect of Irreversible Electroporation on Blood Vessels. Technol Cancer Res Treat 2007;6:255–360. [PubMed: 17668932]
14. Onik G, Mikus P, Rubinsky B. Irreversible electroporation: implications for prostate ablation. Technol Cancer Res Treat 2007;6:295–300. [PubMed: 17668936]
15. Rubinsky B, Onik G, Mikus P. Irreversible electroporation: a new ablation modality--clinical implications. Technol Cancer Res Treat 2007;6:37–48. [PubMed: 17241099]
16. Miller L, Leor J, Rubinsky B. Cancer Cells Ablation with Irreversible Electroporation. Technol Cancer Res Treat 2005;4:699–705. [PubMed: 16292891]
17. Lavee J, Onik G, Mikus P, Rubinsky B. A Novel Nonthermal Energy Source for Surgical Epicardial Atrial Ablation: Irreversible Electroporation. The Heart Surgery Forum 2007;10:E162–E167. [PubMed: 17597044]
18. Al-Sakere B, Andre F, Bernat C, et al. Tumor Ablation with Irreversible Electroporation. PLoS ONE 2007;2:e1135. [PubMed: 17989772]
19. Maor E, Ivorra A, Leor J, Rubinsky B. Irreversible Electroporation Attenuates Neointimal Formation After Angioplasty. IEEE Trans Biomed Eng 2008;55:2268–2274. [PubMed: 18713696]
20. Davalos R, Rubinsky B, Mir L. Theoretical analysis of the thermal effects during in vivo tissue electroporation. Bioelectrochemistry 2003;61:99–107. [PubMed: 14642915]
21. Davalos R, Rubinsky B. Temperature considerations during irreversible electroporation. Int J Heat Mass Transf 2008;51:5617–5622.
22. Wissler EH. Pennes' 1948 paper revisited. J Appl Physiol 1998;85:35–41. [PubMed: 9655751]
23. Jing, Liu; Xu, L. Estimation of blood perfusion using phase shift in temperature response to sinusoidal heating at the skin surface. IEEE Trans Biomed Eng 1999;46:1037–1043. [PubMed: 10493066]
24. Gabriel S, Lau RW, Gabriel C. The dielectric properties of biological tissues: II. Measurements in the frequency range 10 Hz to 20 GHz. Phys Med Biol 1996;41:2251–2269. [PubMed: 8938025]
25. Diller KR, Pearce JA. Issues in Modeling Thermal Alterations in Tissues. Ann N Y Acad Sci 1999;888:153–164. [PubMed: 10842631]
26. Wright NT. On a Relationship Between the Arrhenius Parameters from Thermal Damage Studies. J Biomech Eng 2003;125:300–304. [PubMed: 12751294]
27. Maor E, Ivorra A, Rubinsky B. Non Thermal Irreversible Electroporation: Novel Technology for Vascular Smooth Muscle Cells Ablation. PLoS ONE 2009;4:e4757. [PubMed: 19270746]
28. Hofmann F, Ohnimus H, Scheller C, Strupp W, Zimmermann U, Jassoy C. J Membr Biol 1999;169:103–109. [PubMed: 10341032]
29. Tekle E, Wolfe MD, Oubrahim H, Chock PB. Biochem Biophys Res Commun 2008;376:256–60. [PubMed: 18771656]
30. Piñero J, López-Baena M, Ortiz T, Cortés F. Apoptotic and necrotic cell death are both induced by electroporation in HL60 human promyeloid leukaemia cells. Apoptosis 1997;2:330–336. [PubMed: 14646546]
31. Kong D, Melo LG, Gnecchi M, et al. Cytokine-Induced Mobilization of Circulating Endothelial Progenitor Cells Enhances Repair of Injured Arteries. Circulation 2004;110:2039–2046. [PubMed: 15451799]
32. Chamley-Campbell J, Campbell G, Ross R. Phenotype-dependent response of cultured aortic smooth muscle to serum mitogens. J Cell Biol 1981;89:379–383. [PubMed: 7251658]
33. Koyama H, Raines EW, BornFeldt KE, Roberts JM, Ross R. Fibrillar Collagen Inhibits Arterial Smooth Muscle Proliferation through Regulation of Cdk2 Inhibitors. Cell 1996;87:1069–1078. [PubMed: 8978611]
34. Schulick AH, Taylor AJ, Zuo W, et al. Overexpression of transforming growth factor 1 in arterial endothelium causes hyperplasia, apoptosis, and cartilaginous metaplasia. Proc Natl Acad Sci U S A 1998;95:6983–6988. [PubMed: 9618525]
35. Hruska KA. Vascular Smooth Muscle Cells in the Pathogenesis of Vascular Calcification. Circ Res 2009;104:710–711. [PubMed: 19325156]
36. Speer MY, Yang H, Brabb T, et al. Smooth Muscle Cells Give Rise to Osteochondrogenic Precursors and Chondrocytes in Calcifying Arteries. Circ Res 2009;104:733–741. [PubMed: 19197075]

37. Majesky MW, Lindner V, Twardzik DR, Schwartz SM, Reidy MA. Production of transforming growth factor beta 1 during repair of arterial injury. J Clin Invest 1991;88:904–910. [PubMed: 1832175]

38. Sutra T, Morena M, Bargnoux A, Caporiccio B, Canaud B, Cristol J. Superoxide production: A procalcifying cell signalling event in osteoblastic differentiation of vascular smooth muscle cells exposed to calcification media. Free Radic Res 2008;42:789–797. [PubMed: 19051077]

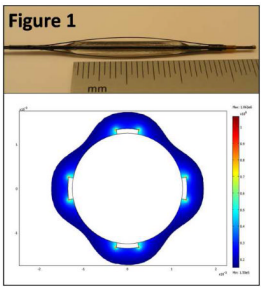

Figure 1. Endovascular NTIRE prototype (top) and finite element simulation of the electric field distribution (bottom)

The image of the endovascular NTIRE prototype (top) shows four nitinol electrodes on top of an inflated balloon. Only the two centimeters along the balloon are exposed and are in direct contact with the blood vessel. The finite element simulation presented here (bottom) is based on a two dimensional simplification of the original geometry. The solution is based on potential difference of 600 volts between the electrodes, and assumes isotropic electric properties. Only electric field values of 1,500 V/cm are shown here, to demonstrate that the entire thickness of the artery is experiencing an electric field high enough to induce irreversible electroporation.

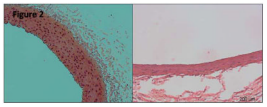

Figure 2. Hematoxylin and Eosin stain (×20) at 7 days

H&E stain (×20 magnification) of a control iliac artery (left) and NTIRE-treated iliac artery after seven days (right), both taken from the same animal. The slide demonstrates the distinct decrease in cellularity of the tunica media at one week (right), with relative decrease in tunica media thickness as well as secondary perivascular inflammation.

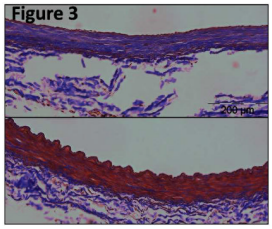

Figure 3. Masson's Trichrome stain at 35 days

Masson's Trichrome stain (×20 magnification) of a control iliac artery (bottom) and NTIRE - treated iliac artery after 35 days (top), both taken from the same animal. Collagen fibrils are in purple color. This figure demonstrates the abundance of collagen fibrils five weeks following IRE-ablation of the arterial wall.

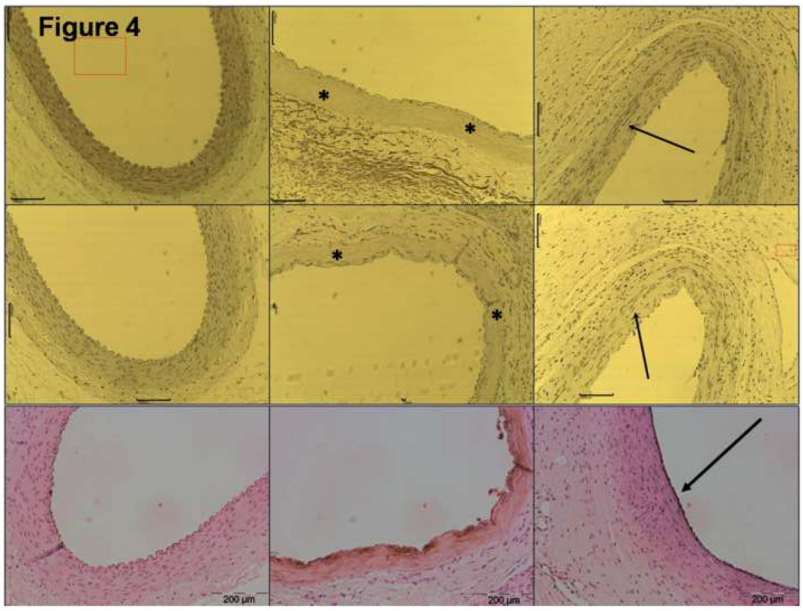

Figure 4. Advanced Immunostainings – control, day 7 and day 35

Top row shows smooth muscle actin immunostaining (×10 magnification) of a control iliac artery (left), and NTIRE -treated arteries at 7 days (middle) and 35 days (right). It demonstrates the absence of vascular smooth muscle cells in the NTIRE-treated arteries compared with the control.Tunica media at day 7 is marked with asterisks and regenerated cellular components at day 35 are marked with an arrow. Middle row shows proliferating cell nuclear antigen immunostaining (×10 magnification) of a control iliac artery (left), and NTIRE -treated arteries at 7 days (middle) and 35 days (right). This figure shows the absence of multiplying cells at 7 days (asterisks), and a relatively active process at 35 days with some cells stain positive (arrow). Lower row shows von willebrand factor immunostaining (×20 magnification) of a control iliac artery (left), and NTIRE -treated arteries at 7 days (middle) and 35 days (right). This figures shows that the endothelial layers at 35 days is regenerated, regular in shape, with the endothelial cells producing the vWF molecule (arrow).

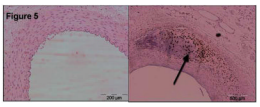

Figure 5. S-100 immunostaining at 35 days

This figure shows a control artery (left) and an IRE-treated artery at 35 days, both stained for the S-100 antigen. The left figure shows one of the few sections with cartilaginous metaplasia with intramural inflammatory process sourrounding it. Immunohistochemisty of S-100 (×20 magnification) stained positive for most of the cells, confirming the cartilaginous characteristics of the process (arrow).

Table 1

Histology results at one and five weeks

This table summarizes the histology results of the treated arteries with respect to both cell ablation and degree of inflammation. With the exception of the first segment of some arteries, which was on the border of the treated segment, all segments demonstrated a significant ablation of VSMC population. For all animals, section #1 is the proximal (closet to the aortic bifurcation) and section #6 is the most distal section. Inflammatory reaction was mild and did not include the entire circumference of the treated arteries. Control arteries (not shown) were unremarkable with no evidence of VSMC population change or any inflammatory process. Section #4 of animal #8 was lost during processing.

		Wall ablation (1 week)		Inflammation (1 week)	
Animal #	Section #	Distribution	Severity	Distribution	Severity
1	1	1	4	2	1
	2	4	4	3	2
	3	4	4	4	2
	4	4	4	2	3
	5, 6	4	4	3	2
2	1	0	0	0	0
	2	2	4	0	0
	3	4	4	4	3
	4	4	4	4	3
	5, 6	4	4	3	4
3	1	4	4	4	1
	2	4	4	3	2
	3	4	4	2	1
	4, 5, 6	4	4	2	1
4	1	1	1	0	0
	2	4	4	4	2
	3, 4, 5, 6	4	4	3	1
		Wall ablation (5 weeks)		Inflammation (5 Weeks)	
Animal #	Section #	Distribution	Severity	Distribution	Severity
5	1	3	4	3	1
	2	4	4	3	1
	3, 4, 5	4	4	4	2

	6	3	4	0	0	0
6	1	3	1	0	0	0
	2–6	4	4	3	1	0
7	1	2	2	0	0	0
	2, 3	4	4	0	0	0
	4	4	4	2	1	0
	5	4	4	0	0	0
	6	3	4	0	0	0
8	1	0	0	0	0	0
	2, 3	4	4	3	1	0
	4	-	-	-	-	-
	5, 6	4	4	0	0	0